Published in: "Light-Emitting Diodes: Materials, Devices and Applications for Solid-State Lighting XVI", Eds. K. P. Streubel, H. Jeon, L.-W. Tu, and N. Linder, Proc. of SPIE, vol. 8278 (2012) 827819

Simulation of light-emitting diodes for new physics understanding and device design

K. A. Bulashevich, O. V. Khokhlev, I. Yu. Evstratov, and S. Yu. Karpov*

STR Group – Soft-Impact, Ltd., P.O.Box 83, 27 Engels av., St.Petersburg, 194156 Russia

Keywords III-nitride LEDs, internal quantum efficiency, efficiency droop, figure of merit, ABC-model, quantum corrections

The paper discusses various factors affecting internal quantum efficiency (IQE) of state-of-the-art III-nitride light-emitting diodes (LEDs). A general figure of merit for LED heterostructures, namely the quality factor, is proposed on the basis of a simple recombination model, which enables comparison of overall performances of the structures either emitting light at different wavelengths or having substantially different designs. The relationships between the quality factor, maximum value of IQE, and IQE droop with the current density are revealed. Some ways for IQE improvement and reducing its droop are considered. Among them, the use of short-period superlattice (SPSL) active regions is found to be quite promising. The operation of such structures and their properties are examined in detail by simulations accounting for quantum corrections to electron and hole transport within the quantum-potential concept.

Preprint 2011

1 Introduction Nowadays, modeling and simulation of III-nitride LEDs has become an important stage of the device design and optimization at leading industrial companies and research centers [1-5]. The simulations cover various aspects of the LED operation, considering electrical, optical, and thermal phenomena in the devices with a certain degree of coupling between them. The factors limiting the internal quantum efficiency and its droop with the operation current, as well as the emission wavelength stability under current variations, are the major points of interest for modeling of LED heterostructures. Suppression of current crowding, reducing the LED series resistance, and accomplishing the highest efficiency of light extraction from the LED die are the principal goals of the chip design. Finally, achieving maximum efficacy at appropriate correlated color temperature and color rendering index and providing high angular uniformity of white light produced by phosphor conversion are the main directions for optimization of LED lamps. All this requires essentially multi-scale and multi-disciplinary approaches to modeling. In addition, non-ordinary properties of III-nitride semiconductors, having no analogs among conventional III-V compounds, need to apply a number of specific physical models in order to simulate adequately operation of III-nitride LEDs [6].

The progress in modeling of III-nitride LEDs in the last decade, problems arising from non-ordinary properties of nitride semiconductors, and still open questions have been recently overviewed in Ref.[6]. In continuation of the review, this paper discusses some new ideas and approaches largely suggested in the recent year. The major focus of the paper is made on the non-thermal efficiency droop in III-nitride LEDs with current and promising ways for solving, at least partly, this problem. Using a simplest ABC-model of carrier recombination in the active region of III-nitride LEDs, we will propose a general figure of merit which enables comparing the LED structures of various designs and those emitting light at different wavelengths. Operation of the LED structures with short-period superlattice (SPSL) active regions that enable substantial reduction in the IQE droop with current is considered by simulation. The importance of quantum effects in the transport of non-equilibrium electrons and holes in such heterostructures is also discussed in the paper.

2 Lessons of ABC-model The simplest ABC-model is based on the following assumptions: (i) there is no electron and hole losses caused by the carrier leakage from the active region of an LED structure, (ii) the non-equilibrium electron and hole concentrations, n and p, in the active region are nearly equal to each other, and (iii) the recombination coefficients A, B, and C (see explanation of their meaning below) are weakly dependent on the carrier concentrations. Then the current density j in the structure and its IQE η are determined by the equations:

Published in: "Light-Emitting Diodes: Materials, Devices and Applications for Solid-State Lighting XVI", Eds. K. P. Streubel, H. Jeon, L.-W. Tu, and N. Linder, Proc. of SPIE, vol. 8278 (2012) 827819

$$\frac{j}{qd} = An + Bn^2 + Cn^3 \quad , \quad \eta = \frac{Bn}{A + Bn + Cn^2} \tag{1}$$

where q is the electron charge, $A = 1/\tau$, τ is the Shockley-Read non-radiative carrier life time, and B and C are the radiative recombination and Auger recombination constants, respectively. The effective width of the recombination region d is normally associated with the total width of the active region. This is definitely correct for a wide active layer. In the case of a single quantum well (SQW), d is nearly equal to the well width extended by the depths of the carrier wave function penetration in the layers cladding the well. In a multi-quantum well (MQW) active region, however, electrons or/and holes may be non-uniformly distributed across the active region. In particular, only one QW may provide a dominant contribution to the carrier recombination in III-nitride LEDs [7,8]. In this case, the width d corresponds just to the effective width of the dominating well.

2.1 Interplay between various recombination channels If the light extraction efficiency (LEE) of an LED is estimated independently either theoretically or on the basis of measurements, one can obtain an experimental dependence $\eta(j)$ from the measured external quantum efficiency (EQE) as a function of operating current. An amazing feature of the ABC-model is that it enables estimating contribution of every particular recombination channel in a wide range of the current density variation. Indeed, if the LED structure satisfies the basic assumptions of the ABC-model, the total current density is the sum of the partial current densities related to radiative (j_{rad}), nonradiative (j_{SR}) and Auger (j_A) recombination. The radiative-recombination current density can be directly obtained from the experimental $\eta(j)$ curve as the product $j_{rad} = j\eta$, since its fraction in the total current density $f_{rad} = j_{rad}/j$ is just equal to η . By plotting η versus j_{rad} , one can determine the radiative current density j_m corresponding to the maximum value of the internal efficiency η_m ($j_m = qdB/\tau C$ within the ABC-model). Then the fractions of Shockley-Read (f_{SR}) and Auger (f_A) recombination currents in the total current density can be found from the equations

$$f_{SR} = j_{SR}/j = \frac{j_m}{j_m + j_{rad}}(1-\eta) \quad , \quad f_A = j_A/j = \frac{j_{rad}}{j_m + j_{rad}}(1-\eta) \tag{2}$$

It is interesting that there is no need to know in Eqs.(2) the width of the recombination region d in order to determine the fractions of various recombination channels in the total current density.

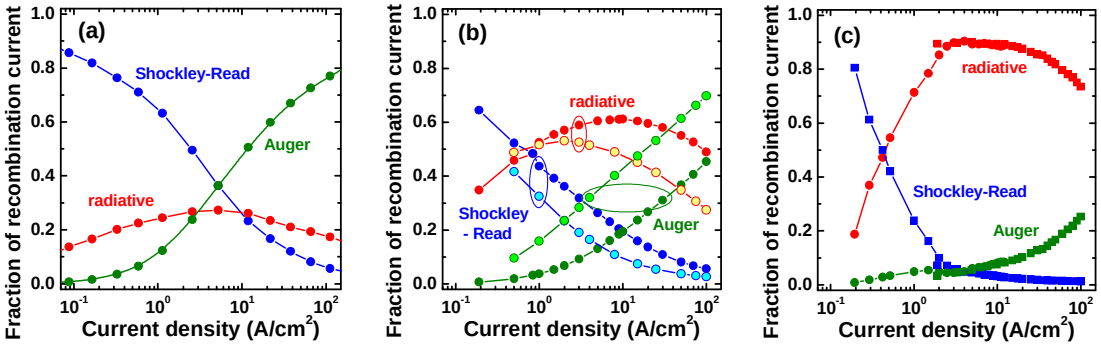

Fig.1 Contributions of various recombination channels to the total current density obtained from the data reported for (a) green SQW structure [9], (b) blue LED structures with MQW (open circles) and SPSL (closed circles) active regions [10], and super-high efficiency blue LEDs operating in CW (circles) and pulsed (squares) modes [11].

Dealing with observable parameters only, Eqs.(2) can be used to estimate contributions of various channels to the total recombination current. Figure 1 displays the fractions of the Shockley-Read, radiative, and Auger recombination currents obtained from the reported data [9-11] for the LED structures of rather low (a), intermediate (b) and super-high (c) efficiency (in the latter case, the compilation of the data for two different LED structures and chips operating at low and high current densities under continuous-wave (CW) and pulsed current pumping, respectively, was used). Such plots are especially helpful for comparison of different structure designs. For instance, Fig.1b provides the results obtained for

Published in: "Light-Emitting Diodes: Materials, Devices and Applications for Solid-State Lighting XVI", Eds. K. P. Streubel, H. Jeon, L.-W. Tu, and N. Linder, Proc. of SPIE, vol. 8278 (2012) 827819

two blue LED structures having either MQW or SPSL active regions [10]. One can see from the figure that contributions of the radiative recombination are comparable with each other in both structures, if the current density is low enough. In contrast, they differ significantly at high current densities where Auger recombination is considerably suppressed in the structure with the SPSL active region, as compared to the MQW one. The mechanism responsible for such suppression is discussed in Sec.3 in detail. As a result, one can expect a smaller efficiency droop with current in the case of the SPSL structure, which is actually observed [10].

2.2 Estimation of recombination constants If one of the recombination constants is known from experiment or calculated theoretically, the ABC-model enables one to find other constants from the experimental dependence $\eta(j)$. We will show this, assuming the recombination constant B to be known, since more or less reliable measurements or theoretical estimates are frequently available just for this parameter. Manipulating with Eqs.(1)-(2), one can obtain for the carrier life time and Auger recombination constant:

$$\tau = \tau_B \frac{f_{\mathrm{rad}}^{1/2}}{f_{\mathrm{SR}}} \quad , \quad C = B^2 \tau_B \frac{f_{\mathrm{A}}}{f_{\mathrm{rad}}^{3/2}} \quad , \quad \text{where } \tau_B = \left(\frac{qd}{jB}\right)^{1/2} \tag{3}$$

Figure 3 shows the carrier life times and Auger recombination constants calculated by Eqs.(3) using the data on four LED structures considered above [9-11]. The calculations accounted for the difference in the recombination region widths d of the structures (in particular, d = 15 nm was assumed for the structure with the SPSL active region, slightly exceeding the total width of their five QWs) and variation of the recombination constant B with the emission wavelength and QW thickness related to the overlapping of the electron and hole wave functions in the wells.

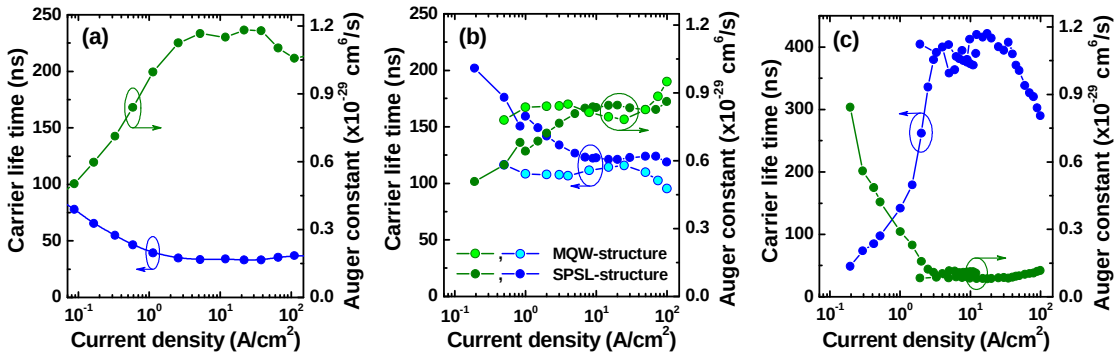

Fig.2 Carrier life times and Auger recombination constants extracted from the data reported for (a) green SQW structure [9] (d = 2.5 nm, B = 1.4×10^{-11} cm^3/s), (b) blue LED structures with MQW (open circles; d = 3 nm, B = 2.0×10^{-11} cm^3/s) and SPSL (closed circles; d = 15 nm, B = 2.6×10^{-11} cm^3/s) active regions [10], and super-high efficiency blue LEDs operating in CW (circles) and pulsed (squares) modes [11] (d = 3 nm, B = 2.6×10^{-11} cm^3/s).

One can see in Fig.3 a wide ranges of the current density where the carrier life times and Auger coefficients are nearly constant, as it is assumed in the ABC-model. Beyond this range, both recombination coefficients vary with the current density, and the ABC-model becomes no longer applicable to analysis of the LED structures. Indeed, the elongation of the electron and hole life times at low current densities can be explained by the impact of carrier localization due to indium composition fluctuations on the rate of non-radiative recombination at threading dislocations [12]. In contrast, decrease of the Auger recombination constant at low current densities cannot be attributed to any physical reason, so it is rather caused by violation of the internal relationships between the strengths of various recombination channels that are inherent in the ABC-model. At high current densities, both recombination constants B and C start to depend on the carrier concentration [13] and, hence, on the current density but there are no evident physical reasons for the carrier life time variation with current.

The range of the ABC-model applicability seen in every plot of Fig.3, where the recombination constants do not vary remarkably with current, corresponds well to the practically important range of the current density variation. This enables comparison of the values of recombination constants for different

Published in: "Light-Emitting Diodes: Materials, Devices and Applications for Solid-State Lighting XVI", Eds. K. P. Streubel, H. Jeon, L.-W. Tu, and N. Linder, Proc. of SPIE, vol. 8278 (2012) 827819

LED structures. For instance, the carrier life times and Auger constants of blue LED structures with SPSL and MQW active layers are nearly the same despite the very different widths of the recombination regions. Moreover, the values of the carrier life times and Auger constants correlate well with the results of differential life time analysis [13,14] reported for the LED structures emitting light in the spectral range of 415-470 nm. Comparison of the blue and green structures (see Fig.3b and Fig.3a, respectively) demonstrates about three times shorter life time in the latter one, which may be attributed to degradation of the materials quality with indium content in the InGaN QWs. Note, that there is no remarkable difference between the Auger recombination constants of the blue and green structures. In the case of super-high efficient blue LEDs (Fig.3c) the calculated carrier life times is nearly four times longer than in the cases of conventional MQW or SPSL structures, which might be explained by a better materials quality. However, the calculated Auger recombination constant is ~7-8 times lower than in other cases considered. The latter result looks somewhat strange, so more experience of ABC-model application to analysis of the recombination constants is required for understanding of the latter result.

2.3 Quality factor as a figure of merit for LED heterostructures One more important feature of the ABC-model is the universal analytical dependence of the predicted IQE on the radiative current density j_{rad}:

$$\eta = \frac{Q}{Q + (j_{\mathrm{rad}} / j_{\mathrm{m}})^{1/2} + (j_{\mathrm{rad}} / j_{\mathrm{m}})^{-1/2}} \tag{4}$$

where Q is the so called quality factor, the dimensionless parameter which is generally defined as $Q = j_{\mathrm{rad}} / (j_{\mathrm{A}} j_{\mathrm{SR}})^{1/2}$. This parameter is independent of the current density and equal to $B(\tau / C)^{1/2}$ within the ABC-model. The quality factor Q increases with the rate of radiative recombination and decreases

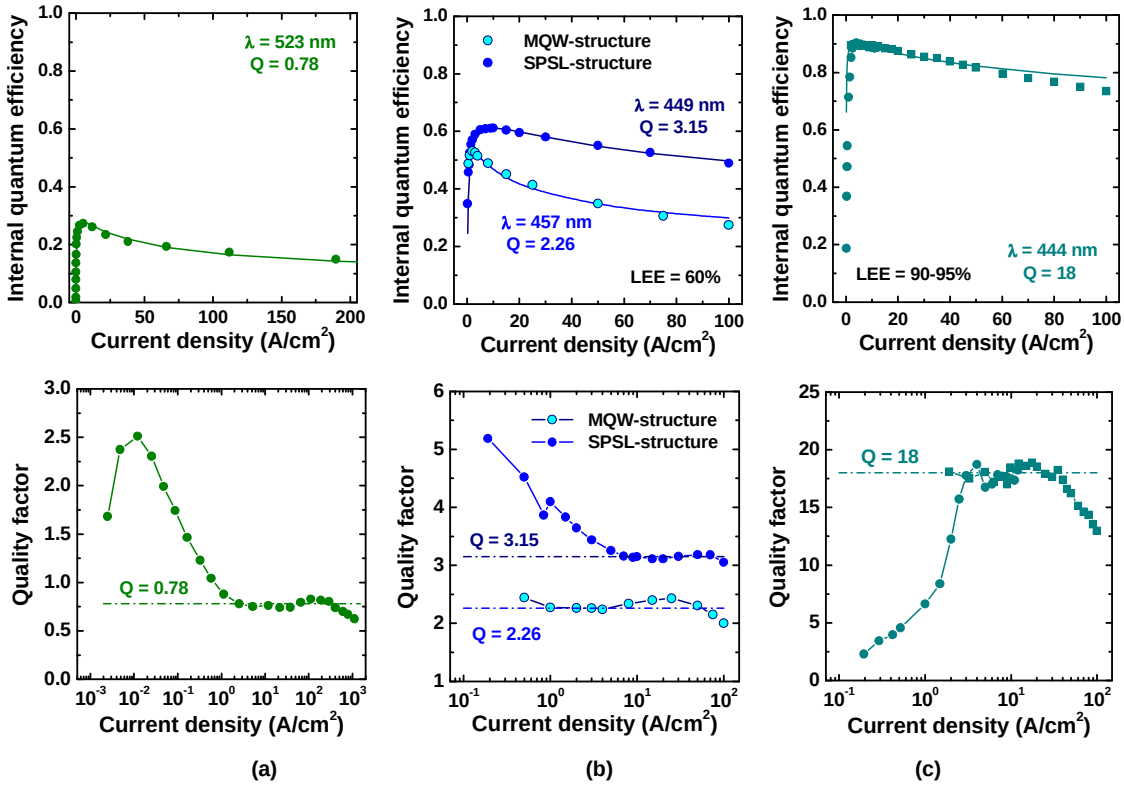

Fig.3 IQE (top) and quality factor (bottom) as a function of current density obtained from the data reported for (a) green SQW structure [9], (b) blue LED structures with MQW and SPSL active regions [10], and super-high efficiency blue LEDs operating in CW (circles) and pulsed (squares) modes [11]. Lines in top plots show the theoretical curves calculated by Eq.(4) with the constant values of the quality factor indicated in bottom plots by dash-dot lines).

Published in: "Light-Emitting Diodes: Materials, Devices and Applications for Solid-State Lighting XVI", Eds. K. P. Streubel, H. Jeon, L.-W. Tu, and N. Linder, Proc. of SPIE, vol. 8278 (2012) 827819

with those of Auger and Shockley-Read recombination. In addition, Eq. (4) shows that not only the maximum IQE, $\eta_m = Q/(Q+2)$, but also the whole IQE dependence on the j_{rad}/j_m ratio is entirely determined by the value of the quality factor. Therefore, this parameter may be considered as a figure of merit for LED structures of various designs or/and emitting light in different spectral ranges.

Top plots in Fig.3 demonstrate that the analytical dependence (4) reproduces quite well the experimental IQE variation with the current density in LED structures of various designs. Both maximum efficiency and its droop with current are found to correlate with the particular value of the quality factor indicated in every plot. This factor varies from 0.78 (low-efficiency green LED structure) to 18 (super-high efficiency blue LED structure), speculating the overall performance of every structure design and materials quality.

Let us come back to the ABC-model applicability for analysis of experimental IQE dependence on the current density or current. The bottom plots in Fig.3 display the quality factors of the above mentioned LED structures *versus* current density calculated from the fractions of the total recombination current displayed in Fig.1. An evident criterion for applicability of the ABC-model is independence of the quality factor of current. One can see that such a criterion is well satisfied by most of the structures in the practically interesting range of the current density variation (~5-100 A/cm^2). The deviation of experimental points to higher values of the *Q*-factor observed in Fig.2a,b at low current densities can be attributed to longer carrier life times due to indium composition fluctuations in InGaN QWs [12]. An opposite deviation of the quality factor from the constant value seen in Fig.2c at low current densities cannot be explained at the moment. However, one should keep in mind that the experimental points plotted in Fig.2c compile the data from different LED chips (and, maybe, different heterostructures) operating under either CW or pulsed injection pumping. This fact may also contribute to the above discrepancy. A slight reduction in the *Q*-factor at high current densities at every bottom plot of Fig.3 may be associated with the device self-heating which is not accounted for in the analysis.

2.4 'Green gap' in the emission efficiency The fact that the green LED structure exhibits a lower *Q*-factor compared to blue structures (Fig.3) is directly related to the so called 'green-gap' problem which implies the IQE reduction in III-nitride LEDs with the emission wavelength λ in the range from ~400 to ~600 nm. Figure 4a demonstrates this trend by the data on maximum EQE collected from various sources and processed in such a way, as to extract the respective IQE values. The data were obtained for C-plane LED structures, except for those grown at UCSB on semipolar planes. The quality factor calculated from the IQE data is plotted in Fig.4b *versus* emission wavelength.

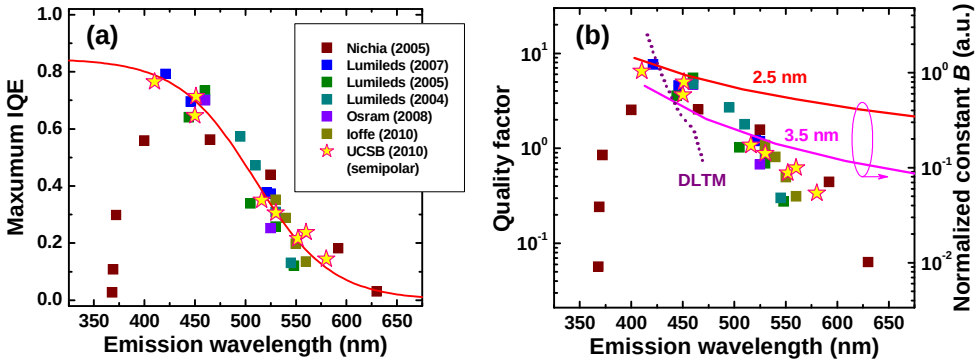

Fig.4 Maximum IQE of various LED structures (a) and corresponding quality factor (b) as a function of LED emission wavelength. Symbols are experimental points compiled from various sources. Line in (a) is a reasonable approximation of the data. Solid lines in (b) are the recombination constants *B* computed for 2.5 nm and 3.5 nm InGaN SQWs. Dotted line in (b) shows the constant *B* obtained by differential life time measurements[14] (DLTM).

Up to now, the mechanism responsible for the IQE reduction with λ (or indium content in InGaN QWs) is not yet completely understood. In this study we have made an attempt to clarify the nature of the 'green gap'. First of all, we noted that a worse materials quality (shorter carrier life time) caused by a higher indium content in the InGaN QWs cannot be a principal reason for a lower *Q*-factor and, hence, lower IQE. Indeed, this would immediately lead to greater values of j_m in green LED structures, as

compared to blue ones. In practice, however, the opposite trend is observed [14]. Then we compared the wavelength variations of the estimated quality factor and calculated recombination constant *B* to which the *Q*-factor is proportional. The constant *B* was calculated for 2.5 nm and 3.5 nm InGaN SQW structures operating at the low current density of 20 A/cm^2 with account of the overlap of electron and hole wave functions (solid lines in Fig.4b). One can see from this comparison that the *Q*-factor decay with λ can be explained by the respective decrease in the recombination constant *B* in the range of 400-510 nm. Such an explanation is consisted with j_m reduction upon increasing the emission wavelength. At the wavelengths longer than ~510 nm, however, the *Q*-factor starts to drop faster than the calculated *B*-constant, which may be the evidence for existence of additional mechanisms lowering the quality factor and, hence, IQE.

Two observations are in conflict with the above explanation. First, the recombination constant *B* estimated from the differential life time measurements [15] (dotted line in Fig.4b) deceases with the wavelength much faster than it is predicted theoretically and even faster than *Q*-factor does by itself. Second, the recombination constant *B* in semipolar LED structures should exhibit much weaker dependence on λ, since there is no built-in polarization field in the QWs, separating the electrons and holes. This, however, is not seen from Fig.4b where the *Q*-factor of the semipolar structures decays very similarly to those of C-plane structures. The discrepancy between the observations and given above explanation of the quality factor dependence on λ points out to some obscure factors limiting IQE of the LED structures at long wavelengths and requiring careful identification in future.

2.5 Ways to improve LED structure performance As shown above, both the maximum IQE of an LED structure and the IQE dependence on the current density are controlled by two parameters: the quality factor *Q* and the radiative current density j_m. So, to achieve the highest IQE of an LED structure one should either increase the *Q*-factor or/and to shift j_m into the practically important range of the current density variation.

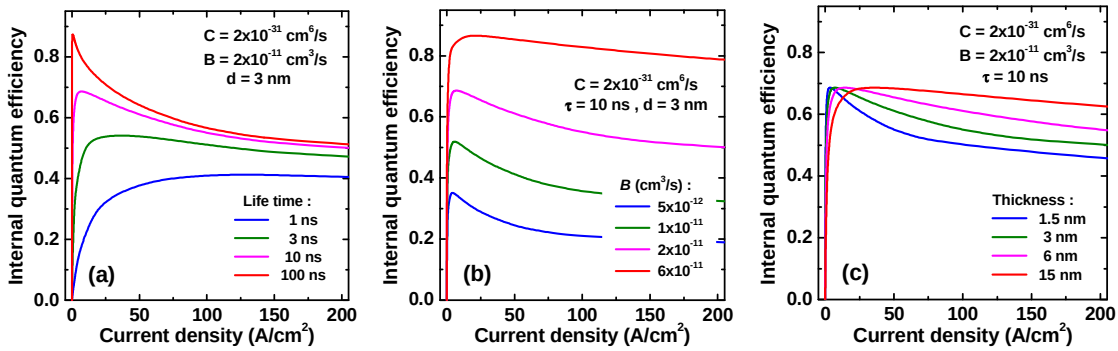

Fig.5 IQE as a function of current density calculated by ABC-model at varied carrier life time (a), radiative recombination constant (b), and recombination region width (c).

One of the evident ways for getting higher IQE is the improvement of materials quality, which leads to a longer carrier life time τ. In terms of the above critical parameters, this increases the *Q*-factor but shifts the current density j_m toward lower values. As a result, the maximum IQE becomes remarkably higher but the efficiency rise in the high-current density region is much less pronounced because of enhanced efficiency droop (Fig.5a). The latter effect can be explained by a rather small contribution of the Shockley-Read channel to the total recombination rate at high current densities (Fig.1). Actually, the improvement of materials quality is more or less effective in the case of initially low IQE, i. e. less than ~0.4-0.5 . At higher initial values, a longer carrier life time produces a rather minor effect on IQE. This means, in particular, that further materials quality improvement cannot be considered as an effective way for the performance improvement in violet and blue LEDs already having a rather high IQE.

Much more remarkable IQE improvement in a wide range of current density variation can be provided by increasing the radiative recombination constant *B* (see Fig.5b). In practice, this can be done by using bandgap engineering of the LED active region [15-17] or exploiting the optical-cavity effects capable of enhancing the spontaneous light emission [18,19]. The former approach seems to be more straightforward and reliable. However, it is interfered by indium surface segregation during MOVPE growth of InGaN QWs, modifying considerably their compositional profile [20] and, eventually, optical properties

Published in: "Light-Emitting Diodes: Materials, Devices and Applications for Solid-State Lighting XVI", Eds. K. P. Streubel, H. Jeon, L.-W. Tu, and N. Linder, Proc. of SPIE, vol. 8278 (2012) 827819

[21]. As for the cavity effects, their impact on LEE has been proved experimentally [22] but the possibility of controlling the spontaneous recombination rate still requires experimental confirmation. It is important that an increase in the constant B results not only in a higher Q-factor and, hence, in a higher IQE maximum but also in a greater j_m, which reduces the efficiency droop (see the upper curve in Fig.5b).

The shift j_m to the practical range of the current density variation can be most easily achieved by enlargement of the recombination region width d. This produces a lower carrier concentration region n in the active and suppresses Auger recombination at high current densities. As a result, the IQE droop becomes much less pronounced at nearly the same value of the IQE maximum (Fig.5c). One of the ways to enlarge d is the use of a wide InGaN active layer, as demonstrated in Ref.[23]. Unfortunately, MOVPE growth of thick InGaN layers still remains problematic because of tendency of this materials to phase separation. Therefore, the above approach is not yet utilized in the LED industry. Generally MQW active regions might provide a wider recombination region but it does not occur because of non-uniform electron/hole injection in the structures with rather thick (larger than ~6-8 nm) barriers separating individual QWs [7,8]. To overcome this problem, the use of SPSL active regions, utilizing very thin barriers between the QWs, has been recently suggested [10,24]. Detailed discussion on advantages of such an approach is given in the next section after short reviewing of quantum corrections to the transport of non-equilibrium electrons and holes.

3 Carrier transport in superlattice active regions and suppression of efficiency droop Conventional drift-diffusion model of the electron and hole transport neglects such quantum effects as tunneling which may become important in thin barriers separating InGaN QWs in the SPSL active layer and/or in the space-charge regions cladding the SPSL layer. This frequently results in underestimated electrical conductivity of MQW LED structures and some other predictions that are not actually take place in practice [6]. On the other hand, application of rigorous quantum-mechanical approaches to the carrier transport based on statistical operator or density matrix is hardly feasible at the moment because of lots of still unsolved problems related to non-locality of electrons and holes, self-consistent description of many-body effects, insufficiently developed quantum theory of carrier scattering, and solution of the governing equations by themselves. So, to improve the above mentioned drawback of the drift-diffusion model we have employed the quantum-potential approach introducing some quantum corrections to the carrier transport model in a simplest way.

3.1 Quantum-potential approach In one of the possible formulations, the quantum-potential approach takes into account the non-local character of the electron and hole interaction with the actual potential formed in a heterostructure (see Fig.6a where the carriers in the conduction and valence bands are schematically represented by wave packets). This can be done by substituting the potential energy of electrons/holes in the conduction/valence band $U(z)$ (hereafter referred to as potential) by the effective potential energy $U_{\text{eff}}(z)$ having a general form [25-27]

$$U_{\text{eff}}(z) = \int_{-\infty}^{\infty} d^3\mathbf{k}\, dz' \cdot G(z - z', \mathbf{k}; \sigma, T) U(z') \tag{5}$$

where $\mathbf{k}$ is the carrier wave vector, G is the core accounting for the carrier interaction with the potential $U(z)$ and being a Gaussian in the simplest case [25,26], parameter $\sigma = \gamma\hbar^2/8m_e k_B T$ is the specific length related to the thermal de Broglie wavelength of the carriers, $\hbar$ is the Plank constant, m_e is the electron/hole effective mass, k_B is the Boltzmann constant, and T is temperature. The length σ appears in the Bohm quantum potential and Wigner-Kirkwood expansion, while the correction factor γ may vary from 2/3 to 3π, depending on particular way of derivation of the quantum potential. Therefore, σ is frequently used as adjustable parameter in practical simulations [26]. We have obtained the value $\gamma = 0.7$ for electrons and holes by fitting their tunneling currents through triangular barriers of various heights. Figures 6b,c show that the quantum-mechanical tunneling current may be well approximated by the quantum-potential model with the correction factor of 0.7, if the barrier is not so high and temperature is not so low.

The effective potential used in the transport equations differs remarkably from the actual one. Figure 7a compares the actual conduction and valence band potentials (solid lines) with the effective potentials (edges of the grey shadow in the plot, which indicates the bandgap) obtained by self-consistent solution of the transport and Poisson equations for 2.5nm $In_{0.2}Ga_{0.8}N$/2.5nm GaN superlattice. One can see that

Published in: "Light-Emitting Diodes: Materials, Devices and Applications for Solid-State Lighting XVI", Eds. K. P. Streubel, H. Jeon, L.-W. Tu, and N. Linder, Proc. of SPIE, vol. 8278 (2012) 827819

the effective potential is much more smooth compared to the actual one. Another feature is that the minima in the effective conduction band edge lie next to the ground electron states in the QWs calculated rigorously by quantum mechanics. A similar but slightly less pronounced correspondence is also observed in the case of holes (the separation of the ground-state energy levels of heavy and light holes is undistinguished in the plot). This fact shows that the quantum-potential approach accounts approximately not only for the carrier tunneling through the MQW barriers but also for the carrier confinement effects in the QWs.

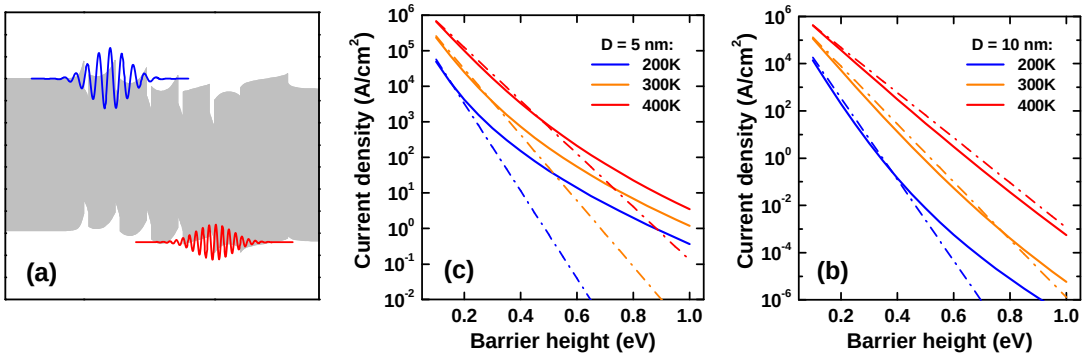

Fig.6 Schematic delocalization of electrons and holes in an LED structure where the bandgap profile is shown by grey shadow (a). Electron tunneling current flowing through the triangular potential barrier with the base D as a function of the barrier height (b,c) calculated at various temperatures by quantum mechanics (solid lines) and by using the quantum-potential approach with the correction factor $\gamma = 0.7$ (dash-dotted lines).

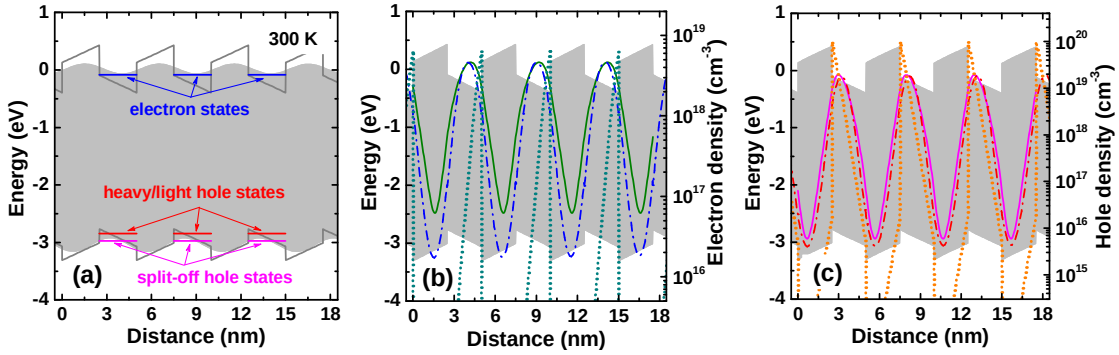

Fig.7 Room-temperature band diagram of the 2.5 nm $In_{0.2}Ga_{0.8}N$/2.5 nm GaN SPSL: grey shadow indicates the quantum-potential bandgap profile used in the transport equations, while solid lines show the actual conduction and valence band alignment; ground electron and hole states obtained from the quantum-mechanical calculations are marked by horizontal lines (a). Distributions of electron (b) and hole (c) densities in the SPSL obtained by quantum mechanics (solid lines), quantum-potential approach with the correction factor $\gamma = 0.7$ for both electrons and holes (dash-dotted lines), and conventional drift-diffusion model (dotted lines). The grey shadow shows here the actual SPSL bandgap profile.

Additional advantage of the quantum-potential approach is more accurate prediction for distributions of electron and hole densities in the LED structures. Figure 7b,c compares the electron and hole densities in the 2.5nm $In_{0.2}Ga_{0.8}N$/2.5nm GaN SPSL structure obtained by rigorous quantum mechanics, quantum-potential approach, and drift-diffusion model. One can see that the carrier penetration from the QWs to the barriers caused by tunneling is rather well reproduced by the quantum-potential model, while the drift-diffusion (classical) approach provides much more sharp carrier density distributions in the wells and extremely low carrier concentrations in the barriers. This is very important for accurate estimations of the radiative and Auger recombination rates that depend non-linearly on the local carrier densities.

Immediate output from the quantum-potential model is more adequate predictions for the current-voltage characteristics of MQW LED structures with high indium content in the QWs. Indeed, the band

diagram of the MQW structure emitting light at 500 nm obtained by conventional drift-diffusion model exhibits a large voltage drop inside the active region accompanied by a step-like band alignment, which favors ballistic electron leakage into the *p*-region of the structure (see Fig.8a). In contrast, the quantum-potential approach provides much more flat band alignment in the heterostructure which would avoid such a leakage (Fig.8b). As a result of the so different band alignments, the I-V characteristics of the LED predicted by drift-diffusion and quantum-potential models differ considerably (Fig.8c). The latter approach provides much more realistic turn-on voltage.

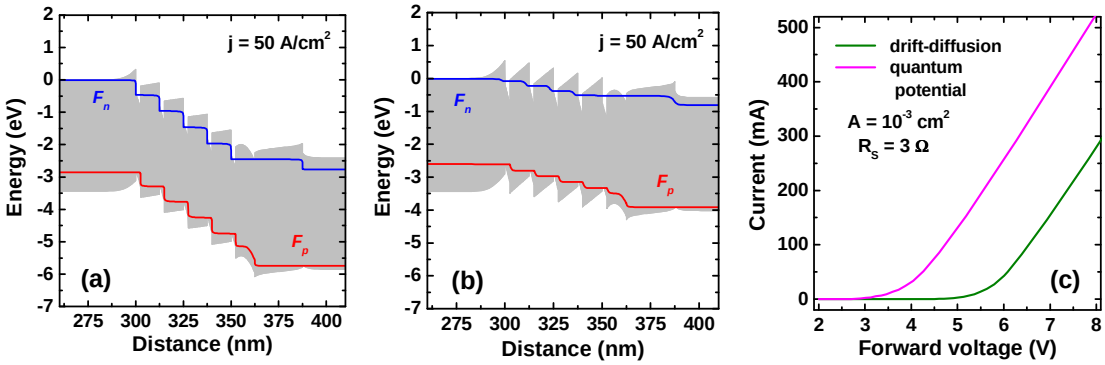

Fig.8 Room-temperature band diagrams of an MQW LED structure emitting light at 500 nm computed by using conventional drift-diffusion (a) and quantum-potential (b) approaches; F_n and F_p are the electron and hole quasi-Fermi levels. Current-voltage characteristics of this structure estimated by these approaches, assuming a certain LED area A and series resistance R_s (c).

3.2 Operation of LED structure with SPSL active region The quantum-potential model of the carrier transport implemented in the SiLENSe 5.2 simulator [28] has been applied to comparative analysis of blue LED structures with either conventional MQW or SPSL active regions [29]. The former one consisted of five 3 nm InGaN QWs separated by 10 nm GaN barriers. The SPSL active layer contained five-period 2.5 nm InGaN/2.5 nm GaN superlattice. Both active regions were unintentionally doped and sandwiched between thick n^+-GaN and *p*-GaN contact layers. In the case of the MQW structure, a 20 nm *p*-$Al_{0.15}Ga_{0.85}N$ electron blocking layer (EBL) was additionally inserted between the active region and *p*-contact layer.

Figure 9a-d compares the band diagrams and distributions of electron and hole densities and radiative recombination rates computed for both LED structures using the quantum-potential approach. In line with the results reported earlier [7,8], electrons and especially holes are very non-uniformly distributed among the individual QWs in the MQW structure, resulting in the fact that only the well adjacent to the *p*-AlGaN EBL gives the major rise to the radiative recombination, i.e. to light emission. This is because of rather wide GaN barriers hindering the hole injection in the remote QWs. In contrast, holes easily penetrate in all the wells in the SPSL active region having much narrower barriers. Moreover, the hole density near the *n*-GaN contact layer is higher than near the *p*-GaN one, while the opposite trend is predicted for electrons. This fact can be explained by uncompensated charges, negative at the *n*-GaN/SPSL and positive at the SPSL/*p*-GaN interface, induced due to the difference between the electric polarization of GaN materials and mean macroscopic polarization of the InGaN/GaN SPSL. The effect is quite similar to that recently studied in the case of a heterojunction formed by two different superlattices [30]. Despite the electron and hole density non-uniformity, the rates of the radiative recombination are nearly the same in all QWs of the SPSL structure. As a result, all the wells provide very comparable contributions to the light emission.

A more uniform distribution of the recombination rate in the SPSL structure (not only of radiative but also of total recombination) actually means an increase of the recombination volume in this structure, as compared to the MQW one. At the same current density, this should lead to lower electron and hole concentrations in the active region. Indeed, the electron density in the SPSL active region is ~1.5 times lower than in the MQW active layer, while the hole peak density differs from that of the MQW structure by a factor of three (see Fig.9a,b). The processing of the experimental data on EQE as a function of operation current (Fig.9e) in a way discussed in Sec.2 shows the parameter j_m to be ~4.5 times greater for the SPSL structure than for MQW one. This is a one more evidence for enlargement of the recombina-

tion volume in the former heterostructure. According to the conclusion made in Sec.2 this should provide a lesser IQE droop at high operation current, which is actually observed experimentally (see Fig.9e).

In addition to the IQE droop suppression, another advantage of the SPSL active region is much higher stability of the emission wavelength with current reported for the first time in Ref.[10] and recently confirmed by simulations [29] (see Fig.9f). Detailed modeling has shown that the major reason for strong blue shift of the emission spectra observed in the MQW structure is the shape modification of the QW adjacent to the *p*-AlGaN EBL upon the bias applied. As just this well primarily contributes to the light emission and lies within the *p*-*n* junction space-charge region, its shape is largely affected by the bias variation, eventually controlling the emission wavelength. In the case of the SPSL structure, only one of five QWs effectively emitting light, which is placed close to the *p*-GaN contact layer, is influenced by the bias variation. This provides a better stability of the emission wavelength of the SPSL structure.

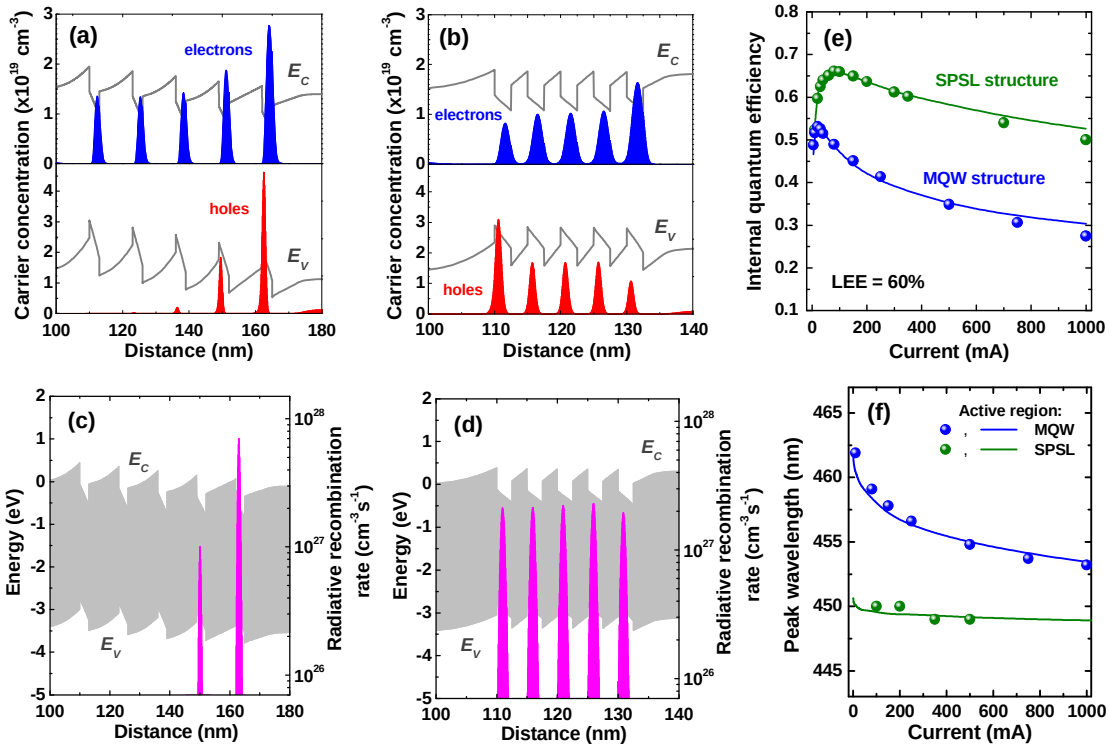

Fig.9 Band diagrams, distributions of carrier densities (a,b) and radiative recombination rates (c,d) in blue (450-460 nm) LED structures with MQW (a,c) and SPSL (b,d) active regions at the current density of 200 A/cm^2. IQE (e) and peak emission wavelength (f) of both structures as a function of current: symbols are experimental points [29], while lines are simulations.

3 Summary Using a simple ABC-model, we have suggested a general figure of merit, the quality factor, which enables one to compare performances of various LED structures. This parameter is directly related to the maximum value of IQE: the greater the *Q*-factor, the higher is IQE. Much more interesting is that the quality factor also determines the whole IQE dependence on the current density, along with the parameter j_m which is the radiative current density corresponding to the IQE maximum. In other words, the *Q*-factor can be also employed to quantify the IQE droop with the current density, as discussed below.

Commonly the droop, $[\eta_m - \eta(j)]/\eta_m$, is measured with respect to IQE/EQE maximum η_m at a certain current I or current density j chosen rather arbitrarily (in the case of commercial LEDs, the operation current normally serves for this purpose). Such a choice may be reasonable for optimization of a particular device structure and chip design but it becomes rather useless for comparing performances of different heterostructures and chips, first of all, because of the difference in the recombination volumes that are specific for each kind of LED. On the other hand, there is a natural measure of the current density or current used for the droop estimation, namely j_m or the current I_m corresponding to the IQE/EQE maximum. The droop estimation at a certain j/j_m or I/I_m ratio allows one to exclude the recombination vol-

Published in: "Light-Emitting Diodes: Materials, Devices and Applications for Solid-State Lighting XVI", Eds. K. P. Streubel, H. Jeon, L.-W. Tu, and N. Linder, Proc. of SPIE, vol. 8278 (2012) 827819

ume from consideration, thus comparing different LED structures under quite similar operation conditions. In this case, i.e. at a chosen ratio $R = j/j_m$, , the efficiency droop is entirely determined by the value of the quality factor, as it can be seen from the equation

$$\frac{\eta_m - \eta(R)}{\eta_m} = \frac{R^{1/2} + R^{-1/2} - 2}{Q + R^{1/2} + R^{-1/2}} \quad , \quad R = j/j_m = I/I_m \tag{6}$$

The higher the *Q*-factor, the lower is the efficiency droop, according to Eq.(6). So, in view of the droop, the quality factor also serves as a figure of merit for the LED structure performance.

Analysis of the *Q*-factor constituents enables assessment of various ways for IQE increasing. We have argued that improvement of the materials quality, resulting in a longer carrier life times, is not an effective approach in the case of violet and blue LEDs operating at the current densities higher than ~30-40 A/cm^2. This is because Auger recombination rather than Shockley-Read recombination is the mechanism limiting IQE under such operation conditions. In contrast, enhancing the radiative recombination *via* proper bandgap engineering and enlarging the recombination volume in the LED structures may be quite promising for the IQE improvement. In particular, the latter approach can be applied by using an SPSL active region with ultra-thin barriers separating InGaN QWs.

To account, at least approximately, such effects as tunneling and quantum confinement essential for operation of LED structures with ultra-thin barriers and QWs, a quantum-potential approach has been invoked. Compared to conventional drift-diffusion model, this approach provides more accurate predictions for the overall band alignment and electron and hole density distributions in the LED structures, as well as for their current-voltage characteristics.

Using the quantum-potential approach, we have compared the operation of LED structures with conventional MQW and SPSL active regions. Design of the latter structure is found to provide effective increase in the recombination volume due to more uniform redistribution of electrons and holes injected in the active region among the individual QWs. As expected, this results in suppression of the efficiency droop with current. Additional advantage of the SPSL LED structure is better stability of the emission wavelength under current variations.

'Green gap' in the efficiency of III-nitride LEDs has been considered in terms of the *Q*-factor. We have found a correlation between the *Q*-factor reduction and decrease in the calculated radiative recombination constant with the emission wavelength in the spectral range of ~410-510 nm (at longer wavelength, the *Q*-factor decayed faster than the recombination constant). The correlation found implies that the slowdown of the radiative recombination with the wavelength caused by the quantum-confined Stark effect may be a mechanism responsible, at least partly, for the 'green gap'. The above interpretation is, on the one hand, in conflict with the *Q*-factor reduction observed in semipolar LED structures where the built-in polarization field is absent. On the other hand, it is supported by the differential life-time measurements [14] provided much faster decrease of the radiative recombination constant with the wavelength than it has been predicted theoretically. These contradictions require more detailed and systematic studies, both experimental and theoretical, to understand better the nature of the 'green gap'.

References

[1] Sabathil, M., Laubsch, A., and Linder, N., "Self-consistent modeling of resonant PL in InGaN SQW LED-structure", Proc. SPIE, 6486, 64860V-1-9 (2007).

[2] Park, E.-H., Nicol, D., Kang, H., Ferguson, I. A., Jeon, S.-K., Park, J.-S., and Yoo, T.-K., "The effect of silicon doping in the selected barrier on the electroluminescence of InGaN/GaN multi quantum well light emitting diodes", Appl. Phys. Lett., 90, 031102 (2007).

[3] López, T. and Margalith, T., "Electro-Thermal Modelling of High Power Light Emitting Diodes Based on Experimental Device Characterization", Proc. Comsol Conference 2008, Boston MA, October 9-11 (2008).

[4] Han, S.-H., Lee, D.-Y., Lee, S.-J., Cho, C.-Y., Kwon, M.-K., Lee, S. P., Noh, D. Y., Kim, D.-J., Kim, Y. C., and Park S.-J., "Effect of electron blocking layer on efficiency droop in InGaN/GaN multiple quantum well light emitting diodes", Appl. Phys. Lett., 94, 231123 (2009).

[5] Lobo, N., Rodriguez, H., Knauer, A., Hoppe, M., Einfeldt, S., Vogt, P., Weyers, M., and Kneissl, M., "Enhancement of light extraction in ultraviolet light-emitting diodes using nanopixel contact design with Al reflector", Appl. Phys. Lett., 96, 081109 (2010).

[6] Karpov, S. Yu., "Modeling of III-nitride Light-Emitting Diodes: Progress, Problems, and Perspectives", Proc. SPIE, 7939, 79391C-1-12 (2011).

[7] David, A., Grundmann, M. J., Kaeding, J. F., Gardner, N. F., Mihopoulos, T. G., and Krames, M. R., "Carrier distribution in (0001)InGaN/GaN multiple quantum well light-emitting diodes", Appl. Phys. Lett., 92, 053502 (2008).
[8] Bulashevich, K. A., Ramm, M. S., and Karpov, S. Yu., "Assessment of various LED structure designs for high-current operation", Phys. Stat. Solidi (c), 6, S804-S806 (2009).
[9] Laubsch, A., Sabathil, M., Bergbauer, W., Strassburg, M., Lugauer, H., Peter, M., Lutgen, S., Linder, N., Streubel, K., Hader, J., Moloney, J. V., Pasenow, B. and Koch, S. W., "On the origin of IQE 'droop' in InGaN LEDs", Phys. Stat. Solidi (c), 6, S913-S916 (2009).
[10] Zakheim, D. A., Pavluchenko, A. S., and Bauman, D. A., "Blue LEDs – way to overcome efficiency droop", Phys. Stat. Solidi (c), 8, 2340-2344 (2011).
[11] Narukawa, Y., Ichikawa, M., Sanga, D., Sano, M., and Mukai, T., "White light emitting diodes with super-high luminous efficacy", J. Phys. D: Appl. Phys., 43, 354002 (2010).
[12] Karpov, S. Yu., "Effect of localized states on internal quantum efficiency of III-nitride LEDs", Phys. Stat. Solidi RRL, 4, 320-322 (2010.
[13] David, A. and Grundmann, M., "Droop in InGaN light-emitting diodes: A differential carrier lifetime analysis", Appl. Phys. Lett., 96, 104504 (2010).
[14] David, A. and Grundmann, M., "Influence of polarization fields on carrier lifetime and recombination rates in InGaN-based light-emitting diodes", Appl. Phys. Lett., 97, 033501 (2010).
[15] Arif, R. A., Ee, Y.-K., and Tansu N., "Polarization engineering via staggered InGaN quantum wells for radiative efficiency enhancement of light emitting diodes", Appl. Phys. Lett., 91, 091110 (2007).
[16] Son, J. H. and Lee, J.-L., "Strain engineering for the solution of efficiency droop in InGaN/GaN light-emitting diodes", Optics Express, 18, 5466-5471 (2010).
[17] Lee, Y.-J., Chen, C.-H., and Lee, C.-J., "Reduction in the Efficiency-Droop Effect of InGaN Green Light-Emitting Diodes Using Gradual Quantum Wells", IEEE Photon. Technol. Lett., 22, 1506-1508 (2010).
[18] Delbeke, D., Bockstaele, R., Bienstman, P., Baets, R., and Benisty, H., "High-Efficiency Semiconductor Resonant-Cavity Light-Emitting Diodes: A Review", IEEE J. Selected Topics Quantum Electron., 8, 189-206 (2002).
[19] Neogi, A., Lee, C.-W., Everitt, H. O., Kuroda, T., Tackeuchi, A., and Yablonovitch E., "Enhancement of spontaneous recombination rate in a quantum well by resonant surface plasmon coupling", Phys. Rev. B, 66, 153305 (2002).
[20] Talalaev, R. A., (a), Karpov, S. Yu., Evstratov, I. Yu. and Makarov, Yu. N., "Indium Segregation in MOVPE Grown InGaN-Based Heterostructures", Phys. Stat. Solidi (c), 0, 311-314 (2002).
[21] Bulashevich, K. A., Karpov, S. Yu., Yu., Talalaev, R. A., Evstratov, I. Yu., and Makarov, Yu., N., "Segregation effects and bandgap engineering in InGaN quantum-well heterostructures", MRS Symp. Proc., 743, L6.5.1- L6.5.6 (2003).
[22] Shen, Y. C., Wierer, J. J., Krames, M. R., Ludowise, M. J., Misra, M. S., Ahmed, F., Kim, A. Y., Mueller, G. O., Bhat, J. C., Stockman, S. A. and P. S. Martin, "Optical cavity effects in InGaN/GaN quantum-well-heterostructure flip-chip light-emitting diodes", Appl. Phys. Lett., 82, 2221-2223 (2003).
[23] Gardner, N. F., Müller, G. O., Shen, Y. C., Chen, G., Watanabe, S., Götz, W.,and Krames M. R., "Blue-emitting InGaN–GaN double-heterostructure light-emitting diodes reaching maximum quantum efficiency above 200 A/cm2", Appl. Phys. Lett., 91, 243506 (2007).
[24] Ni, X., Li, X., Xie, J., Fan, Q., Shimada, R., Özgür, Ü., and Morkoç, H.., "Reduction of efficiency droop in InGaN-based blue LEDs", Proc. SPIE, 7216, 716W-1-7 (2009).
[25] Feynman R. and Kleinert, H., "Effective classical partition function", Phys. Rev. A, 34, 5080 (1986).
[26] Ferry, D. K., Ramey, S., Shifren, L., and Akis, R., "The Effective Potential in Device Modeling: The Good, the Bad and the Ugly", J. Comput. Electronics, 1, 59-65 (2002).
[27] Ahmed, S. S., Ringhofer, C.,and Vasileska, D., "Parameter-Free Effective Potential Method for Use in Particle-Based Device Simulations", IEEE Trans. Nanotechnology, 4, 465-471 (2005).
[28] http://www.str-soft.com/products/SimuLED/
[29] Zakheim, D. A., Pavluchenko, A. S., Bauman, D. A., Bulashevich, K. A., Khokhlev, O. V., and Karpov, S. Yu., "Efficiency droop suppression in InGaN-based blue LEDs: experiment and numerical modeling", accepted for publication in Phys. Stat. Solidi (a) (2011).
[30] Bulashevich, K. A. and Karpov, S. Yu., "Heterojunctions between group-III nitride short-period superlattices", Phys. Stat. Solidi (c), 2, 2394-2398 (2005).